

Numerical simulation of the double-to-single ionization ratio for the helium atom in strong laser fields

Zhangjin Chen, Yanyan Zheng, Weifeng Yang, and Xiaohong Song

Department of Physics, College of Science, Shantou University, Shantou, Guangdong 515063, People's Republic of China

Junliang Xu and L. F. DiMauro

Department of Physics, The Ohio State University, Columbus, Ohio 43210, USA

Oleg Zatsarinny and Klaus Bartschat

Department of Physics and Astronomy, Drake University, Des Moines, Iowa 50311, USA

Toru Morishita

Institute for Advanced Science and Department of Engineering Science, The University of Electro-communications,

1-5-1 Chofu-ga-oka, Chofu-shi, Tokyo 182-8585, Japan

Song-Feng Zhao

College of Physics and Electronic Engineering, Northwest Normal University, Key Laboratory of Atomic and Molecular Physics and Functional Materials of Gansu Province, Lanzhou 730070, People's Republic of China

C. D. Lin

J. R. Macdonald Laboratory, Physics Department, Kansas State University, Manhattan, Kansas 66506-2604, USA

(Received 5 November 2015; published 29 December 2015)

We present calculations on the ratio between double and single ionization of helium by a strong laser pulse at a wavelength of 780 nm using the quantitative rescattering (QRS) model. According to this model, the yield for the doubly charged ion He^{2+} can be obtained by multiplying the returning electron wave packet (RWP) with the total cross sections (TCSs) for electron impact ionization and electron impact excitation of He^+ in the singlet spin channel. The singlet constraint was imposed since the interaction of the helium atom with the laser and the recollision processes both preserve the total spin of the system. An R -matrix (close-coupling) code is used to obtain accurate TCSs, while the RWPs, according to the QRS, are calculated by the strong-field approximation for high-energy photoelectrons. The laser field, which lowers the required energy for the electron to escape from the nucleus at the time of recollision, is also taken into account. The simulated results are in good agreement with the measured $\text{He}^{2+}/\text{He}^+$ ratio over a broad range of laser intensities. The result demonstrates that the QRS approach based on the rescattering model is fully capable of quantitatively interpreting nonsequential double ionization processes.

DOI: [10.1103/PhysRevA.92.063427](https://doi.org/10.1103/PhysRevA.92.063427)

PACS number(s): 32.80.Fb, 32.80.Rm, 34.50.Rk, 34.80.Dp

I. INTRODUCTION

The phenomenon of nonsequential double ionization (NSDI) of atoms that are exposed to intense laser fields has been the subject of numerous theoretical and experimental studies for more than three decades. Experimentally, the early works began with measurements of the total doubly charged ion yield as a function of the laser intensity [1–4]. The prominent well-known general feature observed in the intensity dependence of the double ionization data is the appearance of a characteristic “knee” structure. This dramatic enhancement of doubly charged ion yields has been explained by the semiclassical rescattering model [5,6]. Since the differential helium double ionization measurement by Weber *et al.* [7] at the turn of this century, many more experiments [8–16] were reported on ion momentum distributions along the laser polarization direction, or momentum correlations between the two outgoing electrons. Most of the two-electron momentum distributions exhibit distinct correlated patterns [10], but anticorrelation structure has also been observed for double ionization close to threshold [17]. Such differential ion

yields provide more detailed insight into the dynamics of laser-electron and electron-electron interaction in the double ionization process. The various measurements have attracted utmost attention by theorists.

Among the theoretical simulations, numerically solving the time-dependent Schrödinger equation (TDSE) [14,18,19] should provide the most accurate results. However, in spite of the rapid increase in computing power during recent years, TDSE calculations for NSDI in intense laser fields at wavelengths around 800 nm or even longer still represent formidable computational challenges, and the numerical accuracy of the predictions is hard to quantify. Even if such pure numerical solutions could be obtained, the results alone would likely not offer much insight into the basic mechanisms for the double ionization processes, such as the role of rescattering and/or other possible pathways. Today, it is generally accepted that rescattering is the main mechanism for NSDI. Based on the S -matrix theory or the strong field approximation (SFA), the rescattering concept is explicitly embedded in the second-order term. It has been used to simulate a variety of NSDI processes,

including the total yield for double ionization [20–22], the momentum distribution of the doubly charged ion [23], and the correlated electron momentum distributions [23–28]. Other calculations have been carried out using classical ensemble theory [29–32] and semiclassical models [33–35], in which tunneling ionization of the first electron is treated quantum mechanically, while the propagation and the collision of the returning electron with the parent ion are treated classically.

The high-precision measurement of the total single and double ionization yields of He in a strong laser pulse at a wavelength of 780 nm reported by Walker *et al.* [4] is of special interest. Many theoretical efforts have been devoted to this problem [21,36–40]. While the *ab initio* time-dependent [36] and *S*-matrix [20–22] calculations show good agreement with the experimental data, early calculations of double ionization probabilities using the recollision model obtained results that were a factor of 50 smaller than the experimental findings [4,37]. This serious disagreement certainly has raised questions about the applicability of the recollision model.

The general validity of the recollision model for NSDI was established by van der Hart and Burnett [39]. They assumed that the electric field from the laser reduces the ionization potential of the singly charged ion core at the instant of rescattering and also considered spin conservation in double ionization of He.

In this paper, we employ the quantitative rescattering (QRS) model [41,42], with the focal-volume averaging included, to simulate the ratio of doubly to singly charged He ions as a function of the laser intensity for a wavelength of 780 nm. The QRS model was originally developed for high-order above-threshold ionization (HATI) [41,43] and high-order harmonic generation [41,44]. It was then applied to simulate the correlated two-electron momentum distributions of rare-gas atoms in NSDI [45–47] as well as the total nonsequential double ionization yield of Ar atoms [48].

The remainder of the present paper is arranged as follows. In Sec. II, we summarize the QRS model for NSDI. In Sec. III, we first calculate the total cross sections (TCSs) for excitation and ionization of He^+ by electron impact and the returning-electron wave packet (RWP). We then discuss how to determine the screening factor introduced in the calculation of the RWP and demonstrate how the presence of an electric field at the time of rescattering affects the total double ionization yield and lowers the threshold intensity.

Unless indicated otherwise, atomic units (a.u.) are used throughout the paper.

II. THEORETICAL MODEL

A. QRS model for NSDI

The key ingredient of the QRS model for HATI is the factorization of the momentum distribution for high-energy photoelectrons with momentum of magnitude p at a detection angle θ with respect to the polarization of the laser field,

$$D(p, \theta) = W(k_r) \frac{d\sigma(k_r, \theta_r)}{d\Omega_r}, \quad (1)$$

where $d\sigma(k_r, \theta_r)/d\Omega_r$ is the elastic electron differential scattering cross section (DCS) with a momentum of magnitude k_r at an angle θ_r with respect to the direction of the returning

electron. The momentum distribution of the returning electrons is described by the wave packet $W(k_r)$. The detected photo-electron momentum \mathbf{p} and the momentum \mathbf{k}_r of the scattered electron are related by

$$\mathbf{p} = \mathbf{k}_r - \mathbf{A}_r, \quad (2)$$

where \mathbf{A}_r is the instantaneous vector potential at the time of recollision. Focusing on high-energy returning electrons that are important for NSDI processes, we use the relation [43]

$$k_r = 1.26|\mathbf{A}_r|. \quad (3)$$

The idea of the QRS model is applicable to all laser-induced rescattering processes. For NSDI, therefore, it is related to impact ionization and excitation of the parent ion by the returning electrons. Assuming that all electrons in the excited states are further ionized by the laser, they contribute to the total yield of doubly charged ions and to the TCS. These TCSs should be weighted by the flux of the incident electron beam, which is described by the RWP. Thus the total NSDI yield is evaluated from

$$\mathcal{Y}^{2+} = \int dE_r [W_L(E_r) + W_R(E_r)][\sigma_{\text{exc}}(E_r) + \sigma_{e2e}(E_r)]. \quad (4)$$

Here E_r is the energy $E_r = k_r^2/2$ of the returning electron, $\sigma_{\text{exc}}(E_r)$ and $\sigma_{e2e}(E_r)$ are the TCSs for electron impact excitation and ionization from the ground state of the target ion, and $W_L(E_r)$ and $W_R(E_r)$ are the volume-integrated wave packets extracted from the “left” ($k_z < 0$) and the “right” ($k_z > 0$) sides of the two-dimensional momentum distributions for HATI photoelectrons, respectively. For long pulses considered here, $W_L(E_r) = W_R(E_r)$.

B. Returning electron wave packet

The RWP can be evaluated using Eq. (1), which may be expressed as

$$W(k_r) = D(p, \theta) / \frac{d\sigma(k_r, \theta_r)}{d\Omega_r}. \quad (5)$$

We emphasize that, in principle, the wave packet should be independent of the scattering angle [41,43]. In this calculation, we took it from scattering at $\theta_r = 170^\circ$.

It has been demonstrated that the RWP obtained from the SFA and the TDSE agree well with each other for the parameters of interest for the present work [43]. Consequently, it is convenient to employ the SFA for the calculation of the RWP, especially in the case of long laser pulses with high intensities, for which TDSE calculations are extremely challenging and time consuming.

Details of the SFA model for HATI of hydrogenlike atoms were presented in Ref. [49]. The depletion effect was not accounted for in that work. However, to accurately calculate the RWP for NSDI of helium by 160-fs, 780-nm laser pulses at intensities as high as $10 \times 10^{14} \text{ W/cm}^2$, the depletion of the ground state of He cannot be neglected. We use a hydrogenlike wave function to describe the ground state of He, which takes the form

$$\Psi_{1s}(\mathbf{r}) = 2Z^{3/2} \exp(-Zr) Y_{00}(\hat{\mathbf{r}}), \quad (6)$$

where $Z = 1.345$ is the effective charge of the ion core. To account for the depletion of the ground state, we introduce the decay factor

$$\beta(t) = \exp \left[- \int_{-\infty}^t dt' W(t')/2 \right]. \quad (7)$$

Here $W(t)$ is the time-dependent modified ADK (Ammosov-Delone-Krainov) [50] rate proposed by Tong and Lin [51]. Therefore, in the SFA model, the ground-state wave function $\Psi_{1s}(\mathbf{r})$ should be replaced by $\Psi_{1s}(\mathbf{r})\beta(t)$.

The potential seen by the returning electron is taken as a Yukawa potential

$$V(\mathbf{r}) = -\frac{Z}{r} e^{-\alpha r}. \quad (8)$$

Here α is a screening parameter introduced to avoid the singularity in the calculation of the amplitude.

Within the SFA, the elastic-scattering amplitude is calculated in the first-order plane-wave Born approximation,

$$f(\mathbf{q}) = -\frac{1}{2\pi} \int \exp(i\mathbf{q} \cdot \mathbf{r}) V(\mathbf{r}) d\mathbf{r}, \quad (9)$$

where \mathbf{q} is the momentum transfer with magnitude

$$q = 2k_r \sin(\theta_r/2). \quad (10)$$

In this model, the elastic-scattering DCS in Eq. (5) can be expressed as

$$\frac{d\sigma(k_r, \theta_r)}{d\Omega_r} = |f(\mathbf{q})|^2. \quad (11)$$

C. Total cross sections for excitation and ionization of He^+

The QRS formulation allows us to employ accurate electron impact excitation and electron impact ionization cross sections, even though the RWP is obtained from a one-electron model. In this work, these cross sections are calculated with the R -matrix method, using our fully parallelized B -spline R -matrix (BSR) code [52]. Details about the method can be found in a recent topical review [53].

Specifically, we set up a 450-state close-coupling model, with 36 states of He^+ below the ionization threshold and the remaining 414 states providing a discretization of the ionization continuum. Using an R -matrix box radius of 50 a.u., the 15 bound states up to principal quantum number $n = 5$ are good representations of the physical bound states, while the remaining 21 states below the ionization threshold are used to approximate the countable but infinite Rydberg spectrum. The highest energy of the pseudostates was 365 eV.

We included target orbitals with orbital angular momentum up to $\ell = 4$ and solved the coupling equations numerically for total orbital angular momenta of the projectile plus target system up to $L = 25$. In order to do so, we expanded all orbitals in a B -spline basis with 114 splines of order 8. The calculation for the external region was performed with a parallelized version of the STGF program [54]. If necessary, a top-up procedure based on the geometric-series approximation was used to estimate the contribution from higher L values.

We then obtained the angle-integrated total cross sections for electron-impact excitation and ionization by summing up the individual cross sections for all states (physical plus

pseudo) below the ionization threshold to obtain an estimate for the excitation contribution and for all the pseudostates above the ionization threshold for ionization. In order to compare with experiment and other calculations (see below), the spin-averaged cross section for unpolarized projectile and target beams is required. This cross section is defined as

$$\sigma(E) = \frac{1}{4}\sigma^s(E) + \frac{3}{4}\sigma^t(E), \quad (12)$$

where E is the projectile energy while the superscripts s (singlet) and t (triplet) indicate the total spin of the system. For the present work, only the singlet cross section is needed, since the laser field does not change the singlet character of the total wave function. That character is determined by the initial $(1s^2)^1S$ state.

III. RESULTS AND DISCUSSION

A. Electron impact excitation and ionization cross sections of He^+

Figure 1 exhibits the TCSs for electron impact excitation of He^+ from the ground state. In addition to the singlet cross section needed for the present work, we also compare the current results for the spin-averaged cross section with the convergent close-coupling (CCC) [55] predictions for the combined excitation of the $n = 2, 3$, and 4 levels. For the quantities given, both the CCC and the present BSR models, with a large number of pseudostates included in the close-coupling expansion, can be considered converged to an overall accuracy of a few percent (most likely even better). Hence, the remaining differences seen are essentially due to the inclusion of the physical $n = 5$ states, plus an estimate for the contribution from the higher Rydberg states, in the BSR model. Figure 1 shows that the singlet excitation cross section is much larger than the spin-averaged cross section below 100 eV, but the difference diminishes quickly at higher energies due to the decreasing importance of electron exchange.

In order to obtain the probability for double ionization, we now consider the TCSs for electron impact ionization of

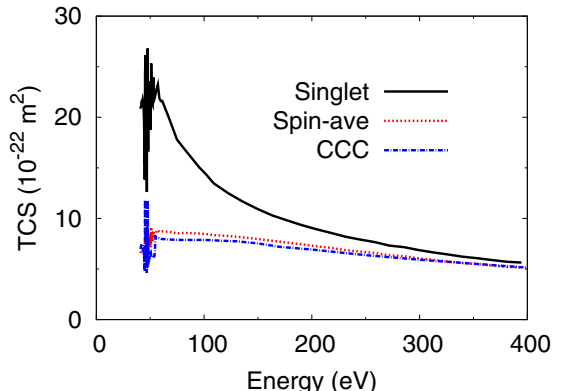


FIG. 1. (Color online) Total cross sections for electron impact excitation of He^+ from the ground state. The present BSR results are given for both the singlet spin channel alone and for the spin-averaged cross section. The latter results are compared with CCC predictions [55] for the combined excitation of the $n = 2, 3$, and 4 levels.

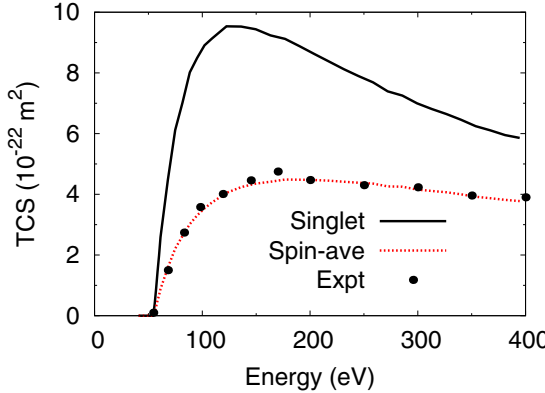


FIG. 2. (Color online) Total cross sections for electron impact ionization of He^+ in the ground state. Results are shown for the singlet spin channel alone and for the spin-averaged cross section. The latter predictions are compared with the experimental data of Peart *et al.* [56].

He^+ . Our results for the singlet spin channel alone and for the spin-averaged case are shown in Fig. 2. We find excellent agreement with the experimental data of Peart *et al.* [56]. This is not surprising, given the many recent successes enjoyed by the pseudostate close-coupling approach, both in the CCC and BSR implementations. Different from electron impact excitation, the singlet TCSs are always more than 1.5 times larger than the spin-averaged ones over the entire energy range considered here. Nevertheless, for both excitation and ionization of He^+ by electron impact, the calculated results show that the proper inclusion of the spin increases the cross sections by about a factor of 2. This, in turn, definitely enhances the ratio between double and single ionization in a strong laser field within the recollision model.

Figure 3 exhibits the singlet TCSs for both electron impact ionization and excitation of He^+ , which are used to simulate the total probability for double ionization. The present BSR predictions are also compared with the corresponding results of van der Hart [38]. It can be seen that the energy dependence of the cross sections for ionization is substantially different from that for excitation. Close to threshold, the ionization

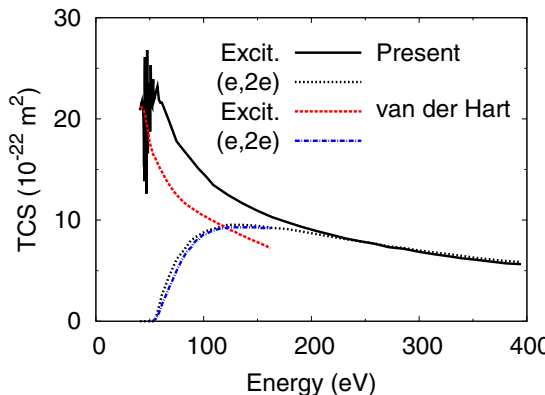


FIG. 3. (Color online) Comparison of the present BRS singlet TCSs for electron impact ionization and excitation of He^+ in the ground state with the corresponding results of van der Hart [38].

cross sections increase rapidly, reaching a maximum just below 150 eV, and then decreasing very slowly with increasing impact energy. On the other hand, the present BSR cross sections for excitation decrease steadily beyond a narrow maximum within about 15 eV above the threshold energy. Around 230 eV, the two cross sections become comparable. The electron impact ionization cross sections of He^+ evaluated by van der Hart [38] are very close to the present BRS results. His excitation cross sections, on the other hand, are significantly smaller than the present ones, since he only considered excitation to $n = 2$.

B. Simulations of the total He^{2+} yields

After accurate spin-singlet TCSs for both excitation and ionization of He^+ have been obtained, together with the RWP below, we are finally ready to combine these ingredients in Eq. (4) to evaluate the total yield for double ionization of He in a strong laser field. The simulated results for the yields of He^{2+} from linearly polarized 780-nm laser pulses as a function of the peak intensity are compared with the experimental data in Fig. 4.

First, we calculate the sequential double ionization yields using the modified ADK model [51] and an improved PPT (Perelomov-Popov-Terent'ev) model [57–59]. Figure 4 reveals that the calculated results underestimate the experimental data by three or even more orders of magnitude at intensities below $2 \times 10^{15} \text{ W/cm}^2$. Since this is the region of interest for the present work, we can safely neglect the contributions from

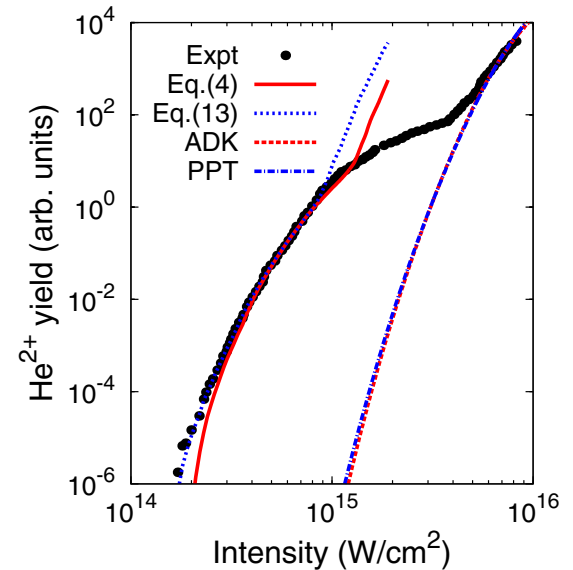


FIG. 4. (Color online) Comparison of the simulated results for the yields of doubly charged ions with the experimental data for He in linearly polarized laser pulses at 780 nm. The solid circles represent the measurements of Walker *et al.* [4], while the dotted and solid curves are the present simulations with and without taking into account the shift of the continuum threshold energy due to the presence of an electric field at the collision time, respectively. The screening factor was set to $\alpha = 1.0$. The simulated results are relative and normalized to the experimental data individually at the intensity of $4.5 \times 10^{14} \text{ W/cm}^2$. The curves on the right are the calculated sequential He^{2+} yields using ADK and PPT.

sequential double ionization in the production of the He^{2+} ions.

The total yields for doubly charged ions He^{2+} based on the QRS model, simulated by using Eq. (4), are also displayed in Fig. 4. The latter results agree very well with the experimental data, except for the low-intensity regime below about $2 \times 10^{14} \text{ W/cm}^2$, and again at higher intensities where the experimental curve begins to flatten out (i.e., in the knee region). For the low-intensity regime, the simulation results lie below the experimental data. For laser-free electron impact excitation and ionization, each process has a threshold energy. In the presence of the laser field, however, the threshold energy is reduced [39]. It should be measured from the top of the potential barrier formed by the asymptotic potential from the Coulomb interaction with the core and from the instantaneous laser field. The maximum of the barrier in the potential $V(z) = zF_r - Z/z$ is $V_b = -2\sqrt{Z|F_r|}$, where F_r is the electric field at the instant of scattering. Furthermore, $Z = 2$ for electron impact ionization and $Z = 1$ for electron impact excitation. The required minimum kinetic energies of the laser-induced returning electron are hence decreased by $\sqrt{2}V_0$ and V_0 (where $V_0 = 2\sqrt{|F_r|}$), respectively, compared to the field-free case.

To account for the shift of the excitation and ionization thresholds at the recollision, we adopt the prescription proposed by van der Hart and Burnett [39], in which the cross sections for ionization and excitation are taken at the field-free energies of $E_r + \sqrt{2}V_0$ and $E_r + V_0$, respectively. Therefore, Eq. (4) is modified to

$$\mathcal{Y}^{2+} = \int dE_r [W_L(E_r) + W_R(E_r)] \times [\sigma_{\text{exc}}(E_r + V_0) + \sigma_{e2e}(E_r + \sqrt{2}V_0)]. \quad (13)$$

The barrier height varies with the time at which the electron returns to the parent ion. In principle, electrons born after the electric field reaches the maximum can return to the origin. For the electric field $F(t) = F_0 \cos(\omega t)$, electrons born at a time before $t_i = 13^\circ/\omega$ return after $t_r = 270^\circ/\omega$ when the electric field is zero. These electrons have a higher ionization rate than those born after $13^\circ/\omega$ and, consequently, dominate the contributions to the RWP. Since accounting for the barrier changes with time in actual numerical computations is very complicated, we chose an “average” returning time of $t_r = 290^\circ/\omega$, which yields the maximum shifts for the threshold energy of 21 and 15 eV, for ionization and excitation, respectively, at a laser peak intensity of $15 \times 10^{14} \text{ W/cm}^2$.

The dotted curve in Fig. 4 represents the yield of He^{2+} ions based on Eq. (13). The inclusion of the threshold shift, indeed, reduces the discrepancy between the model results and the experimental data in the low-intensity region. However, the threshold shift does not improve the model results at higher intensities, as also seen from Fig. 4. This deviation has been traced back to the RWP in the region of low returning energy.

As indicated in Sec. II B, to avoid the singularity due to the asymptotic Coulomb potential in the calculated RWP from the strong-field approximation (the second-order term), a screening parameter was introduced in Eq. (8). In previous calculations, the parameter $\alpha = 1.0$ was used. Figure 5(a)

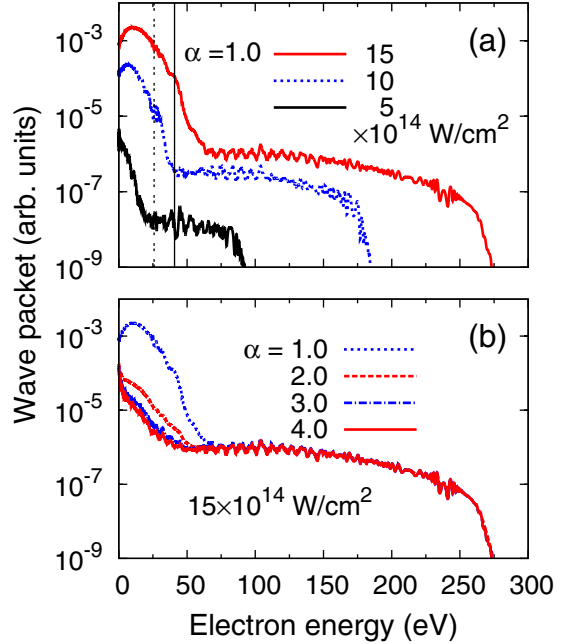


FIG. 5. (Color online) Returning electron wave packets for He in linearly polarized laser pulses at 780 nm. (a) The screening factor is chosen as $\alpha = 1.0$, and the peak intensities are 5, 10, and $15 \times 10^{14} \text{ W/cm}^2$, respectively; (b) The peak intensity is $15 \times 10^{14} \text{ W/cm}^2$ and the screening factors are $\alpha = 1.0, 2.0, 3.0$, and 4.0, respectively. The calculations include integration over the laser focus volume. In (a), the vertical solid line marks the excitation threshold of He^+ in the field-free case, while the vertical dotted line marks the corresponding threshold for excitation in the field at a peak intensity of $15 \times 10^{14} \text{ W/cm}^2$.

shows the RWP for three peak laser intensities. Each RWP starts with a fast drop at low energies before becoming flat in the plateau region, somewhat mimicking ATI spectra. The disagreement between theory and experiment in the high-intensity region originates from the large magnitude of the low-energy distribution in the RWP. Figure 5(b) exhibits the dependence of the RWP on different screening parameters at a peak intensity of $1.5 \times 10^{15} \text{ W/cm}^2$. We see that the RWP in the low-energy region is stabilized for $\alpha \geq 2.0$. When the excitation threshold is shifted down by the laser field, the low-energy part of the RWP contributes more to double ionization. In Fig. 5(b), the $\alpha = 1.0$ curve lies orders of magnitude above the converged results. Consequently, the error in the low-energy RWP is responsible for the overestimate by the model results.

Figure 6 shows how the model calculations converge to the experimental data as α is increased. The inset of this figure depicts the ratio of ionization with respect to excitation for the production of He^{2+} ions as a function of the peak laser intensity. We emphasize that focal-volume averaging has been included in the calculations of the RWP and that the screening factor does not affect the RWP in the plateau region. Recently, the divergence in the rescattering amplitude caused by the Coulomb rescattering was removed by adding the depletion rate of the ground state in the energy denominator [60]. However, this treatment causes the rescattering process to dominate direct ionization.

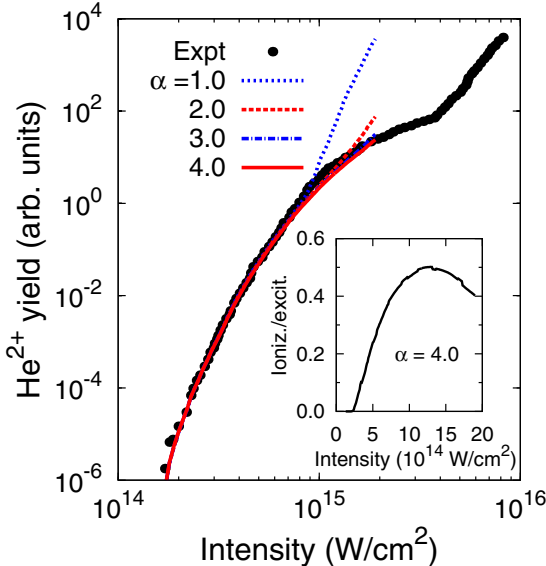


FIG. 6. (Color online) Comparison of the simulated results, with the shift of the continuum threshold energy taken into account, for the yields of doubly charged ions with the experimental data for He in linearly polarized laser pulses at 780 nm. The solid circles represent the measurements of Walker *et al.* [4], while the lines are simulated results for $\alpha = 1.0, 2.0, 3.0$, and 4.0 , respectively. The theoretical predictions are relative and were normalized to the experimental data at the peak intensity of $4.5 \times 10^{14} \text{ W/cm}^2$ with a fixed factor for each screening factor. The inset shows the ratio of the contributions to double ionization from ionization and excitation.

C. Simulation of double-to-single ionization ratio

To obtain the ratio of double-to-single ionization for He subjected to a 160-fs pulse at 780 nm as a function of peak intensity, we also need to evaluate the total probability for single ionization of He. SFA calculations were performed for laser intensities up to $2.0 \times 10^{15} \text{ W/cm}^2$, and the results are found to be in very good agreement with the experimental data, as illustrated in Fig. 7. The ADK and PPT results are also shown in Fig. 7 for comparison. Both the ADK and PPT calculations agree with the data at high intensities, but the ADK curve falls below the measured yield at low intensities. In contrast, the PPT results are in agreement with experiment over the entire intensity range depicted. Again, in all theoretical calculations for single ionization of He, focal-volume averaging was included for each peak intensity. Among the three types of simulation, only the SFA was used to get the ratio of double-to-single ionization, because the QRS model, which was employed to predict the total yield of the doubly charged ion, is based on the SFA model. Since current experiments only provide relative ionization yields as a function of laser intensity, the agreement of the PPT and SFA results with the experimental data only means that the relative laser intensity dependence is predicted correctly. The ADK model starts to show deviations around $4.0 \times 10^{14} \text{ W/cm}^2$.

Experimentally the ionization ratio $\text{He}^{2+}/\text{He}^+$ is the easiest to measure and also the most reliable observable. Among theoretical calculations, the SFA, PPT, and ADK all involve some approximations. In particular, the He^{2+}

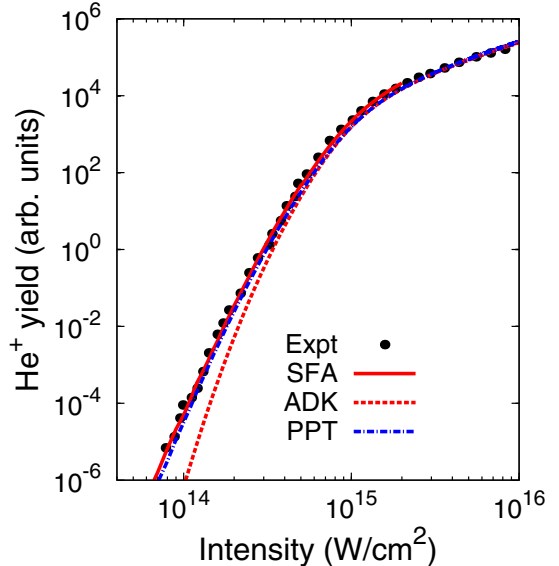


FIG. 7. (Color online) Comparison of theoretical simulations based on SFA, ADK, and PPT with the experimental data for single ionization of He in linearly polarized laser pulses at 780 nm. The solid circles represent the measurements of Walker *et al.* [4]. The theoretical results are normalized individually for the best visual agreement with experiment.

yields were calculated using the rescattering model, with the RWP obtained from the (second-order) strong-field approximation. Since the ratio between rescattering and direct ionization is not correctly reproduced by the SFA, it is necessary to employ the TDSE solutions to calibrate the SFA calculations.

In Fig. 8, we compare the energy spectra between the SFA and TDSE calculations for HATI of He in a 5-cycle, 800-nm laser pulse at the peak intensity of $1.8 \times 10^{14} \text{ W/cm}^2$. The details of the SFA and TDSE calculations were presented previously in Refs. [49,61,62]. Note that our TDSE calculations are based on the single active electron approximation. Figure 8(a) shows that the ionization probabilities predicted by the SFA are much smaller than the TDSE results for both direct ionization and ionization by rescattering. When the SFA spectra are renormalized by a factor of $\eta = 40$ to the TDSE results at high energies, the low-energy spectra of the SFA exceed the TDSE results, as shown in Fig. 8(b). For this specific case, the total probabilities for single ionization of He obtained from SFA and TDSE are $\mathcal{Y}_{\text{SFA}}^+ = 3.26 \times 10^{-8}$ and $\mathcal{Y}_{\text{TDSE}}^+ = 2.44 \times 10^{-7}$, respectively. A factor $\xi = \eta \mathcal{Y}_{\text{SFA}}^+ / \mathcal{Y}_{\text{TDSE}}^+ = 5.3$ should thus be used to correct the ratio between rescattering and direct ionization reproduced by the SFA. Consequently, the double-to-single ionization ratio was calculated according to

$$R = \xi \frac{\mathcal{Y}^{2+}}{\mathcal{Y}_{\text{SFA}}^+}. \quad (14)$$

Here \mathcal{Y}^{2+} is the total yield for NSDI of He from Eq. (13), in which the screening factor in the RWP calculations is set to be $\alpha = 4.0$, and $\mathcal{Y}_{\text{SFA}}^+$ is the total yield for single ionization of He from the SFA. Since the TDSE calculations are very time

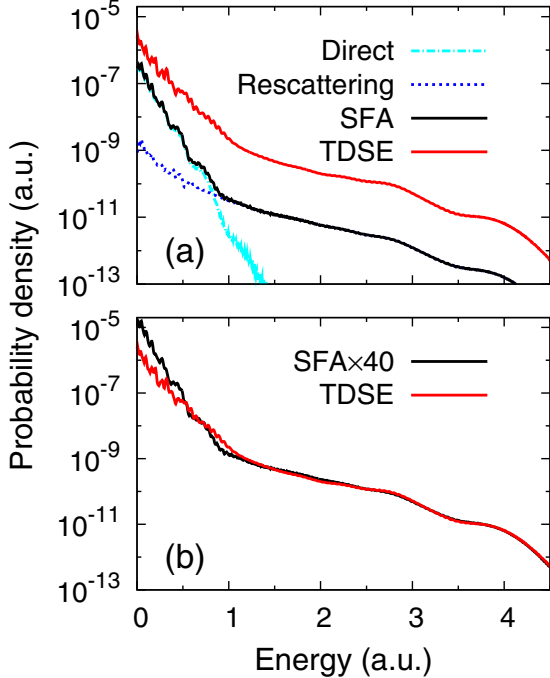


FIG. 8. (Color online) Comparison of energy spectra from the SFA and TDSE calculations for high-order above-threshold ionization of He in a 5-cycle, 800-nm laser pulse at a peak intensity of $1.8 \times 10^{14} \text{ W/cm}^2$.

consuming, we only chose a very short pulse in the calculation for the comparison. The above recipe assumes that the factor ξ does not change significantly with either the laser intensity or the pulse duration.

Figure 9 shows the double-to-single ionization ratio of He as a function of laser intensity from experiment [4] and the results from our calculation as well as three other theoretical attempts in the literature [21,39,40]. Among the theoretical simulations, the *S*-matrix approach [21] generally predicts ratios less than half the experimental values. This model does not include

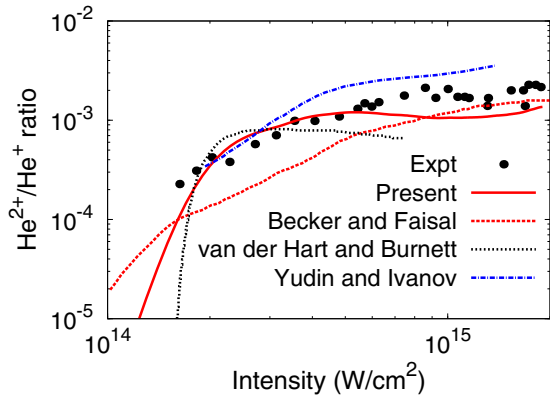


FIG. 9. (Color online) Ratio between double and single ionization of He as a function of intensity for a 160-fs pulse with a wavelength of 780 nm. The present simulations are compared with the experimental data of Walker *et al.* [4], as well as other theoretical results of Becker and Faisal [21], van der Hart and Burnett [39], and Yudin and Ivanov [40].

contributions from electron impact excitation processes, and the electron impact ionization cross section was obtained from the Lotz formula [63]. van der Hart and Burnett [39] used a different recollision model, while the cross sections for ionization and excitation to the $n = 2$ states were also calculated by the *R*-matrix method. They, too, only included the singlet cross sections. Their results for the double-to-single ionization ratio as a function of laser intensity are in fair agreement with experiment. In the simulation of Yudin and Ivanov [40], accurate singlet scattering cross sections from the CCC approach [55] were used. Their results suggest that the ratio increases monotonically with increasing laser intensity.

The comparison of the present calculations with the experimental data in Fig. 9 appears to be very satisfactory. The drop-off of the ratio in the low-intensity tail shown from this calculation follows the trend of the experimental data. At higher intensities, our calculated ratios also exhibit a small decrease before slowly increasing again. Although the trend is consistent with the experimental data, the position of the change is not at the correct intensity. Nevertheless, in light of the strong nonlinearity of the processes involved, the remaining small discrepancy seems acceptable.

IV. CONCLUSIONS

We have presented a careful numerical simulation for the double-to-single ionization ratio of He in the nonsequential double ionization region based on the quantitative rescattering (QRS) model. The QRS model has been employed to describe high-energy above-threshold ionization (HATI) photoelectron spectra and high-order harmonic generation (HHG) extensively in the past few years. While QRS has been applied to NSDI processes in our previous publications, it was limited by the lack of accurate electron impact excitation and electron impact ionization cross sections. This restriction is no longer severe with respect to the helium target. In the present work, therefore, we applied the QRS model to test its predictions against the well-known ratios of double-to-single ionization reported by Walker *et al.* [4]. With the field-free electron impact excitation and ionization cross sections accurately calculated by a sophisticated *R*-matrix code and the returning wave packets (RWP) obtained within the strong-field approximation, we were able to identify corrections that are needed to obtain good agreement with the available experimental data. Specifically, it is necessary to account for the lowering of the ionization and excitation thresholds in the presence of the laser field and to introduce a screening factor to calculate the low-energy portion of the returning electron wave packet correctly. These issues did not arise in previous HATI and HHG studies, since those involved only the high-energy portion of the RWP. With these additional modifications, the QRS model was able to reproduce the experimental results reported by Walker *et al.* [4]. The effect of a variable intensity distribution inside the laser focus volume was also included in our simulation. This is relatively straightforward within the QRS theory, since the collision data do not depend on the laser intensity and the RWP can be calculated quickly using the strong-field approximation.

Additional differential NSDI measurements, including ion momentum distributions along the direction of the laser polarization or the correlated two-electron momentum distributions, may provide further insight into the role of electron-electron and electron-laser interactions in the NSDI and also the sequential double ionization regimes. It is desirable that such measurements be carried out at a few intensities, even though this will be experimentally challenging since the double ionization yields drop very quickly with decreasing intensity. Furthermore, similar measurements at different wavelengths, or in two-color laser fields, would be desirable. In spite of recent progress in the calculation of accurate excitation and ionization cross sections for more complex atomic targets (see, for example, Ref. [53]), we recommend that the experiments be performed on He if possible. Alternative targets might be Ne and Ar. Accurate excitation and ionization cross sections were recently generated over a wide range of incident energies for the neutral atoms [64,65], and hence we expect the corresponding calculations for the ions to be relatively straightforward.

ACKNOWLEDGMENTS

This work was supported by the National Natural Science Foundation of China (Grants No. 11274219, No. 11374202, and No. 11274220), the STU Scientific Research Foundation for Talents, and the Scientific Research Foundation for the Returned Overseas Chinese Scholars, State Education Ministry. J.X. was supported by U.S. DOE/BES Contract No. DE-FG02-06ER15833. L.F.D. was supported by U.S. NSF Grant No. PHY-1304218. O.Z. and K.B. were supported by the U.S. National Science Foundation under Grants No. PHY-1430245 and No. PHY-1520970 as well as the XSEDE Allocation No. PHY-090031. T.M. was supported in part by JSPS KAKENHI Grants No. 26400415 and No. 10500598. S.F.Z. was supported by the National Natural Science Foundation of China (Grant No. 11164025). C.D.L. was supported in part by Chemical Sciences, Geosciences and Biosciences Division, Office of Basic Energy Sciences, Office of Science, U.S. Department of Energy.

-
- [1] A. L'Huillier, L. A. Lompre, G. Mainfray, and C. Manus, *Phys. Rev. Lett.* **48**, 1814 (1982); *Phys. Rev. A* **27**, 2503 (1983).
 - [2] D. N. Fittinghoff, P. R. Bolton, B. Chang, and K. C. Kulander, *Phys. Rev. Lett.* **69**, 2642 (1992).
 - [3] B. Walker, E. Mevel, B. Yang, P. Breger, J. P. Chambaret, A. Antonetti, L. F. DiMauro, and P. Agostini, *Phys. Rev. A* **48**, R894 (1993).
 - [4] B. Walker, B. Sheehy, L. F. DiMauro, P. Agostini, K. J. Schafer, and K. C. Kulander, *Phys. Rev. Lett.* **73**, 1227 (1994).
 - [5] K. J. Schafer, B. Yang, L. F. DiMauro, and K. C. Kulander, *Phys. Rev. Lett.* **70**, 1599 (1993).
 - [6] P. B. Corkum, *Phys. Rev. Lett.* **71**, 1994 (1993).
 - [7] Th. Weber, M. Weckenbrock, A. Staudte, L. Spielberger, O. Jagutzki, V. Mergel, F. Afaneh, G. Urbasch, M. Vollmer, H. Giessen, and R. Dörner, *Phys. Rev. Lett.* **84**, 443 (2000).
 - [8] Th. Weber, H. Giessen, M. Weckenbrock, G. Urbasch, A. Staudte, L. Spielberger, O. Jagutzki, V. Mergel, M. Vollmer, and R. Dörner, *Nature (London)* **405**, 658 (2000).
 - [9] R. Lafon, J. L. Chaloupka, B. Sheehy, P. M. Paul, P. Agostini, K. C. Kulander, and L. F. DiMauro, *Phys. Rev. Lett.* **86**, 2762 (2001).
 - [10] B. Feuerstein, R. Moshammer, D. Fischer, A. Dorn, C. D. Schröter, J. Deipenwisch, J. R. Crespo Lopez-Urrutia, C. Höhr, P. Neumayer, J. Ullrich, H. Rottke, C. Trump, M. Wittmann, G. Korn, and W. Sandner, *Phys. Rev. Lett.* **87**, 043003 (2001).
 - [11] E. Eremina, X. Liu, H. Rottke, W. Sandner, A. Dreischuh, F. Lindner, F. Grasbon, G. G. Gaulus, H. Walther, R. Moshammer, B. Feuerstein, and J. Ullrich, *J. Phys. B* **36**, 3269 (2003).
 - [12] R. Moshammer, J. Ullrich, B. Feuerstein, D. Fischer, A. Dorn, C. D. Schröter, J. R. Crespo López-Urrutia, C. Höhr, H. Rottke, C. Trump, M. Wittmann, G. Korn, K. Hoffmann, and W. Sandner, *J. Phys. B* **36**, L113 (2003).
 - [13] M. Weckenbrock, D. Zeidler, A. Staudte, Th. Weber, M. Schöfeller, M. Meckel, S. Kammer, M. Smolarski, O. Jagutzki, V. R. Bhardwaj, D. M. Rayner, D. M. Villeneuve, P. B. Corkum, and R. Dörner, *Phys. Rev. Lett.* **92**, 213002 (2004).
 - [14] A. Staudte, C. Ruiz, M. Schöfeller, S. Schössler, D. Zeidler, Th. Weber, M. Meckel, D. M. Villeneuve, P. B. Corkum, A. Becker, and R. Dörner, *Phys. Rev. Lett.* **99**, 263002 (2007).
 - [15] A. Rudenko, V. L. B. de Jesus, Th. Ergler, K. Zrost, B. Feuerstein, C. D. Schröter, R. Moshammer, and J. Ullrich, *Phys. Rev. Lett.* **99**, 263003 (2007).
 - [16] Y. Liu, S. Tschuch, A. Rudenko, M. Dürr, M. Siegel, U. Morgner, R. Moshammer, and J. Ullrich, *Phys. Rev. Lett.* **101**, 053001 (2008).
 - [17] Y. Liu, D. Ye, J. Liu, A. Rudenko, S. Tschuch, M. Dürr, M. Siegel, U. Morgner, Q. Gong, R. Moshammer, and J. Ullrich, *Phys. Rev. Lett.* **104**, 173002 (2010).
 - [18] J. S. Parker, L. R. Moore, D. Dundas, and K. T. Taylor, *J. Phys. B* **33**, L691 (2000).
 - [19] J. S. Parker, B. J. S. Doherty, K. T. Taylor, K. D. Schultz, C. I. Blaga, and L. F. DiMauro, *Phys. Rev. Lett.* **96**, 133001 (2006).
 - [20] A. Becker and F. H. M. Faisal, *J. Phys. B* **29**, L197 (1996).
 - [21] A. Becker and F. H. M. Faisal, *J. Phys. B* **32**, L335 (1999).
 - [22] A. Becker and F. H. M. Faisal, *Phys. Rev. A* **59**, R1742 (1999).
 - [23] A. Becker and F. H. M. Faisal, *Phys. Rev. Lett.* **84**, 3546 (2000).
 - [24] A. Becker and F. H. M. Faisal, *Phys. Rev. Lett.* **89**, 193003 (2002).
 - [25] C. Figueira de Morisson Faria, H. Schomerus, X. Liu, and W. Becker, *Phys. Rev. A* **69**, 043405 (2004).
 - [26] C. Figueira de Morisson Faria, X. Liu, and W. Becker, *Phys. Rev. A* **69**, 021402(R) (2004).
 - [27] T. Shaaran, M. T. Nygren, and C. Figueira de Morisson Faria, *Phys. Rev. A* **81**, 063413 (2010).
 - [28] X. L. Hao, J. Chen, W. D. Li, B. Wang, X. Wang, and W. Becker, *Phys. Rev. Lett.* **112**, 073002 (2014).
 - [29] S. L. Haan, L. Breen, A. Karim, and J. H. Eberly, *Phys. Rev. Lett.* **97**, 103008 (2006).
 - [30] S. L. Haan, J. S. Van Dyke, and Z. S. Smith, *Phys. Rev. Lett.* **101**, 113001 (2008).
 - [31] C. Huang, Y. Zhou, Q. Zhang, and P. Lu, *Opt. Express* **21**, 11382 (2013).

- [32] Z. Zhang, L. Bai, and J. Zhang, *Phys. Rev. A* **90**, 023410 (2014).
- [33] D. F. Ye, X. Liu, and J. Liu, *Phys. Rev. Lett.* **101**, 233003 (2008).
- [34] D. F. Ye and J. Liu, *Phys. Rev. A* **81**, 043402 (2010).
- [35] A. Emmanouilidou, *Phys. Rev. A* **83**, 023403 (2011).
- [36] J. B. Watson, A. Sanpera, D. G. Lappas, P. L. Knight, and K. Burnett, *Phys. Rev. Lett.* **78**, 1884 (1997).
- [37] B. Sheehy, R. Lafon, M. Widmer, B. Walker, L. F. DiMauro, P. A. Agostini, and K. C. Kulander, *Phys. Rev. A* **58**, 3942 (1998).
- [38] H. W. van der Hart, *J. Phys. B* **33**, L699 (2000).
- [39] H. W. van der Hart and K. Burnett, *Phys. Rev. A* **62**, 013407 (2000).
- [40] G. L. Yudin and M. Yu. Ivanov, *Phys. Rev. A* **64**, 035401 (2001).
- [41] T. Morishita, A.-T. Le, Z. Chen, and C. D. Lin, *Phys. Rev. Lett.* **100**, 013903 (2008).
- [42] C. D. Lin, A.-T. Le, Z. Chen, T. Morishita, and R. Lucchese, *J. Phys. B* **43**, 122001 (2010).
- [43] Z. Chen, A.-T. Le, T. Morishita, and C. D. Lin, *Phys. Rev. A* **79**, 033409 (2009).
- [44] A.-T. Le, R. R. Lucchese, S. Tonzani, T. Morishita, and C. D. Lin, *Phys. Rev. A* **80**, 013401 (2009).
- [45] Z. Chen, Y. Liang, and C. D. Lin, *Phys. Rev. Lett.* **104**, 253201 (2010).
- [46] Z. Chen, Y. Liang, and C. D. Lin, *Phys. Rev. A* **82**, 063417 (2010).
- [47] Z. Chen, Y. Liang, D. H. Madison, and C. D. Lin, *Phys. Rev. A* **84**, 023414 (2011).
- [48] S. Micheau, Z. Chen, A.-T. Le, and C. D. Lin, *Phys. Rev. A* **79**, 013417 (2009).
- [49] Z. Chen, T. Morishita, A.-T. Le, and C. D. Lin, *Phys. Rev. A* **76**, 043402 (2007).
- [50] M. V. Ammosov, N. B. Delone, and V. P. Krainov, *Zh. Eksp. Teor. Fiz.* **91**, 2008 (1986).
- [51] X. M. Tong and C. D. Lin, *J. Phys. B* **38**, 2593 (2005).
- [52] O. Zatsarinny, *Comput. Phys. Commun.* **174**, 273 (2006).
- [53] O. Zatsarinny and K. Bartschat, *J. Phys. B* **46**, 112001 (2013).
- [54] N. Badnell, *J. Phys. B* **32**, 5583 (1999); see also http://amdpp.phys.strath.ac.uk/UK_RmAX/codes.html.
- [55] I. Bray, CCC-database, <http://atom.curtin.edu.au/CCC-WWW/index.html>.
- [56] B. Peart, D. S. Walton, and K. T. Dolder, *J. Phys. B* **2**, 1347 (1969).
- [57] A. M. Perelomov, V. S. Popov, and M. V. Terent'ev, *Sov. Phys. JETP* **24**, 207 (1967).
- [58] S. V. Popruzhenko, V. D. Mur, V. S. Popov, and D. Bauer, *Phys. Rev. Lett.* **101**, 193003 (2008).
- [59] S.-F. Zhao, A.-T. Le, C. Jin, X. Wang, and C. D. Lin (unpublished).
- [60] L. Guo, S. S. Han, X. Liu, Y. Cheng, Z. Z. Xu, J. Fan, J. Chen, S. G. Chen, W. Becker, C. I. Blaga, A. D. DiChiara, E. Sistrunk, P. Agostini, and L. F. DiMauro, *Phys. Rev. Lett.* **110**, 013001 (2013).
- [61] T. Morishita, Z. Chen, S. Watanabe, and C. D. Lin, *Phys. Rev. A* **75**, 023407 (2007).
- [62] Z. Guo, Z. Chen, and X. Zhou, *Chin. Phys. B* **23**, 043201 (2014).
- [63] W. Lotz, *Z. Phys.* **216**, 241 (1968).
- [64] O. Zatsarinny and K. Bartschat, *Phys. Rev. A* **85**, 062710 (2012).
- [65] O. Zatsarinny, Y. Wang, and K. Bartschat, *Phys. Rev. A* **89**, 022706 (2014).